

Electronic Supplementary Information

Bridged Ov-Ru-O-Co coordination induced by Co^{2+δ} substitution in Co/RuO₂ Catalysts for Enhanced Alkaline Hydrogen and Oxygen Evolution

Weijia Guo,^{a,b} Zhan Wang,^a Yangdong Zhou,^c Tongde Wang,^d Gaoming Zhu,^e Farid Akhtar,^f Payam Ahmadian Koudakan,^g Baojing Zhang,^a Jiangmin Jiang, *^a Shuaijun Pan*^{gh} and Peizhong Feng*^a

School of Materials Science and Physics, China University of Mining and Technology, Xuzhou 221116, China.

E-mail: pzfeng@cumt.edu.cn; jmjiang326@cumt.edu.cn

School of Chemical Engineering and Technology, China University of Mining and Technology, Xuzhou 221116, China

School of Chemistry and Chemical Engineering, Chongqing University, Daxuecheng South Road 55, Chongqing 401331, China

Shanghai Key Laboratory of Special Artificial Microstructure Materials and Technology, Key Laboratory of Road and Traffic Engineering of the Ministry of Education, Tongji University, Shanghai 200092, China

Institute of Material and Process Design, Helmholtz-Zentrum Hereon, 21502, Geesthacht, Germany

Division of Materials Science, Luleå University of Technology, 97187 Luleå, Sweden

State Key Laboratory of Chemo/Biosensing and Chemometrics, Hunan Polyimide Film Engineering Technology Research Center, and College of Chemistry and Chemical Engineering, Hunan University, Changsha 410082, China. E-mail: pansj@hnu.edu.cn

Department of Chemical Engineering, The University of Melbourne, Parkville, VIC 3010, Australia

†Electronic supplementary information (ESI) available.

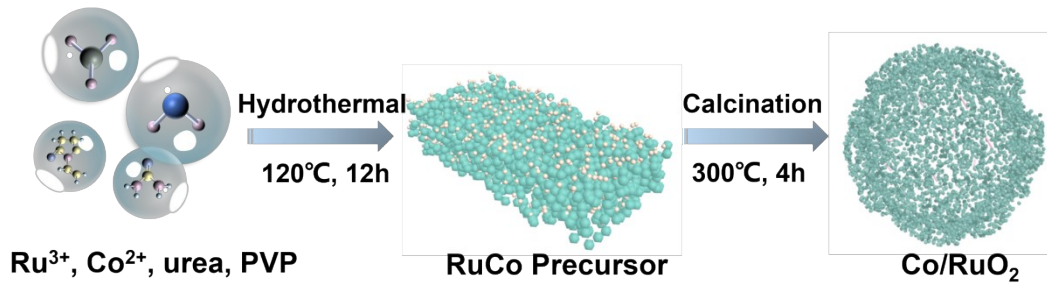


Figure S1. The synthesis process and the microstructure model of products.

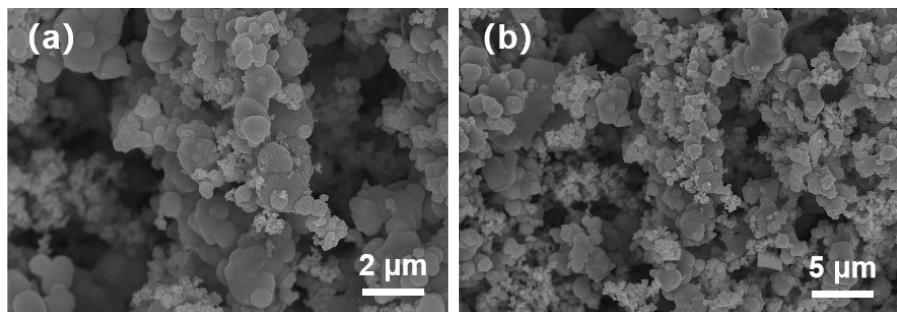


Figure S2. FESEM images of RuCo-based precursors.

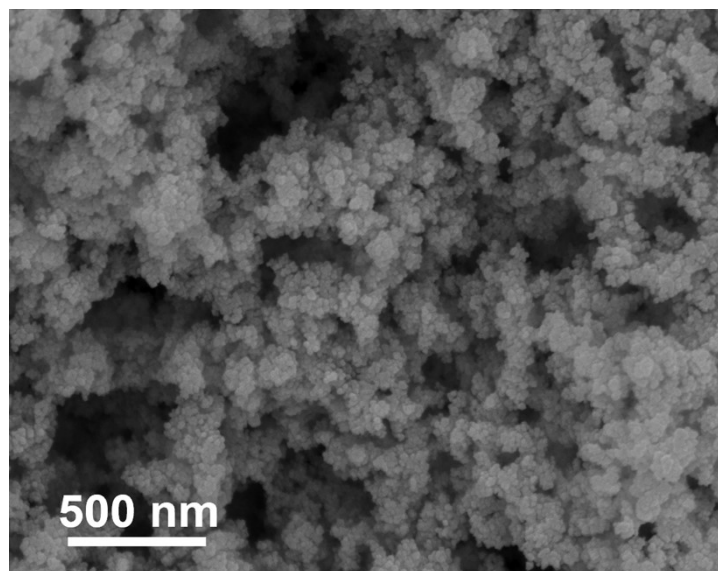


Figure S3. FESEM image of Co/RuO₂-50/1.

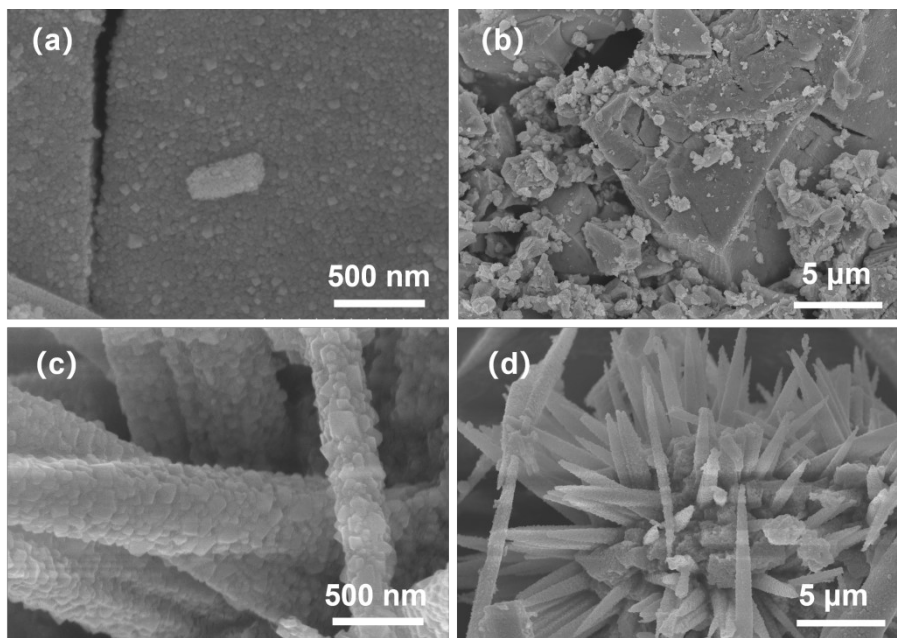


Figure S4. FESEM images of (a,b) RuO₂ and (c,d) Co₃O₄.

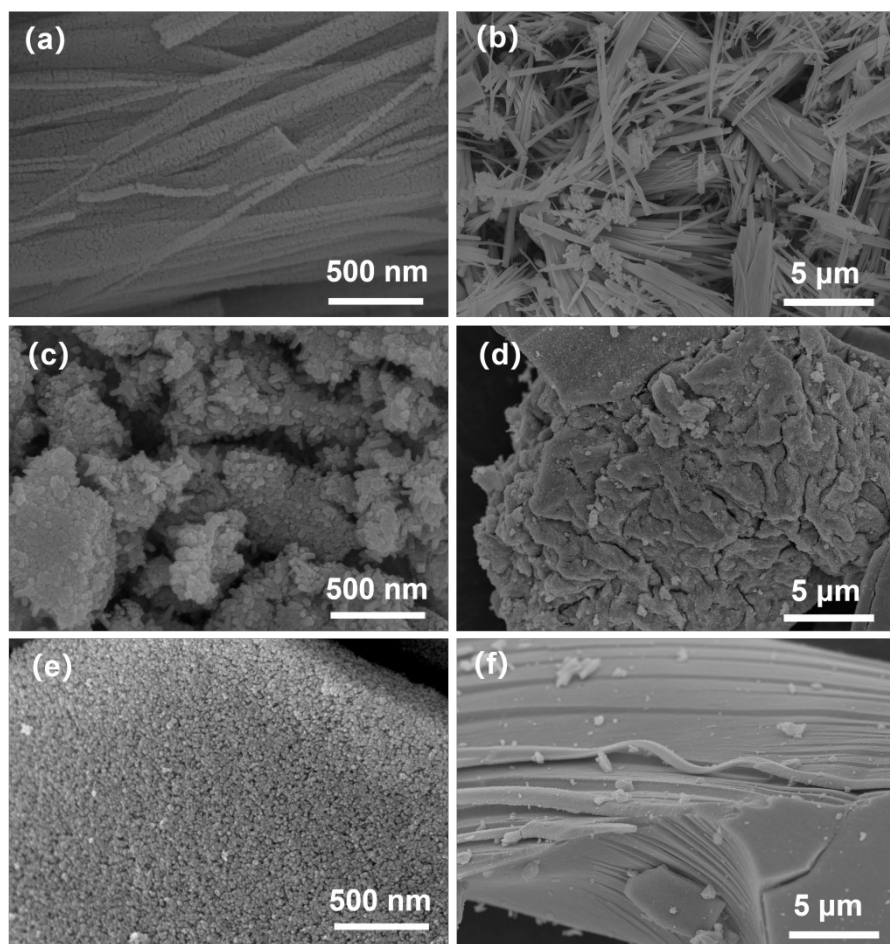


Figure S5. FESEM images of (a,b) Co/RuO₂-50/1, (c,d) Co/RuO₂-1/10 and (e,f) Co/RuO₂-1/20.

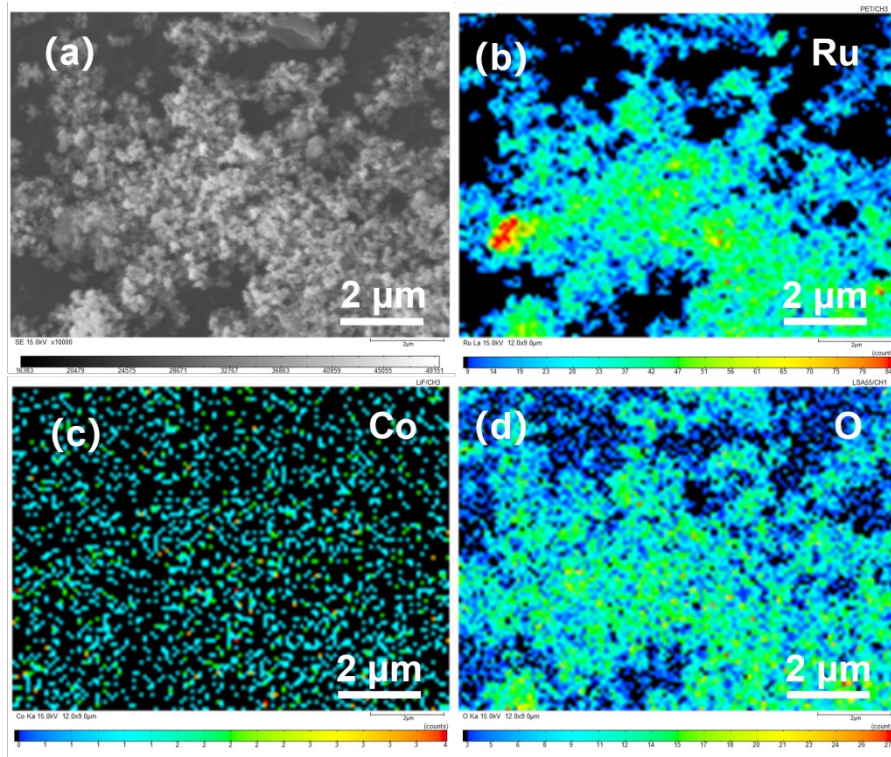


Figure S6. EPMA analysis of Co/RuO₂-1/50.

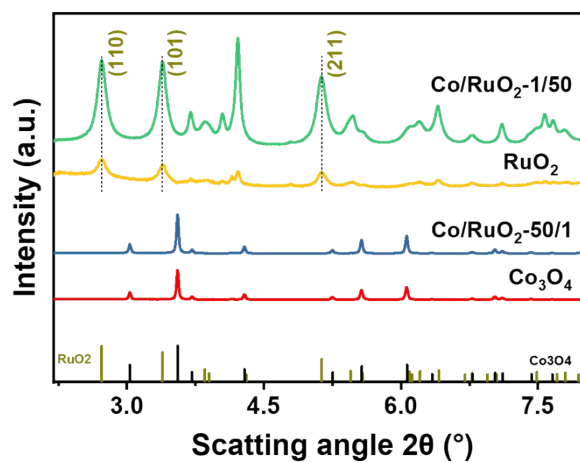


Figure S7. The 1D WAXS profiles of samples corresponding to the 2D WAXS patterns of Fig. 1g.

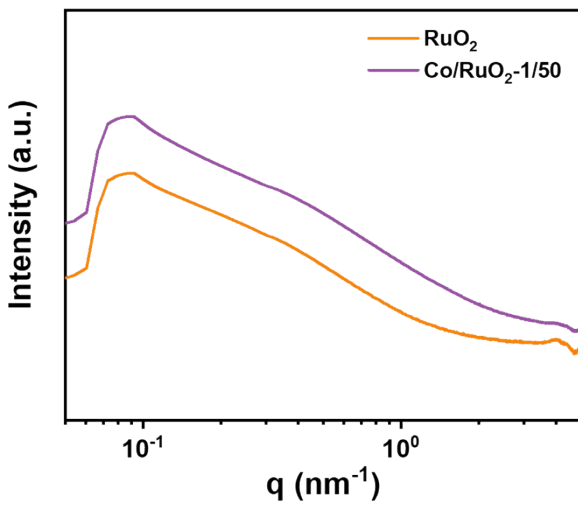


Figure S8. X-Ray scattering curves of RuO_2 and $\text{Co}/\text{RuO}_2\text{-}1/50$ in the SAXS region.

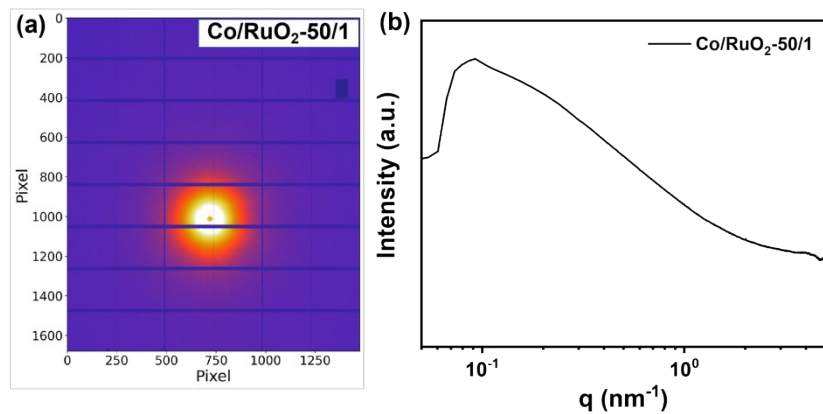


Figure S9. X-Ray scattering curves in the SAXS region of $\text{Co}/\text{RuO}_2\text{-}50/1$ (a) 2D profile, (b) 1D curve.

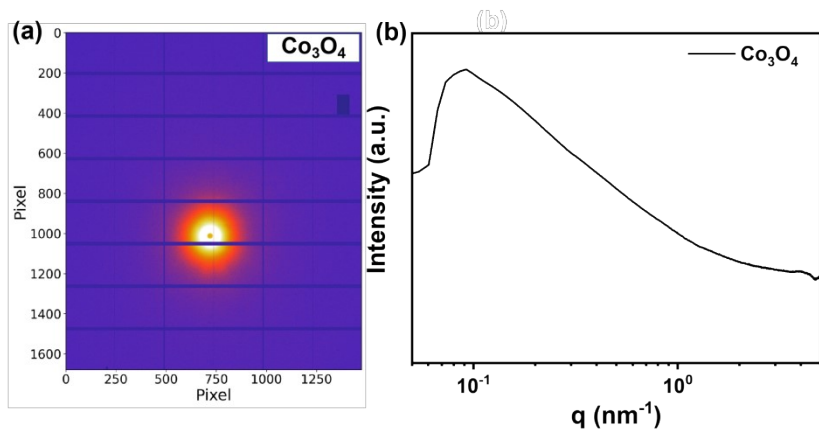


Figure S10. X-Ray scattering curves in the SAXS region of Co_3O_4 (a) 2D profile, (b) 1D curve.

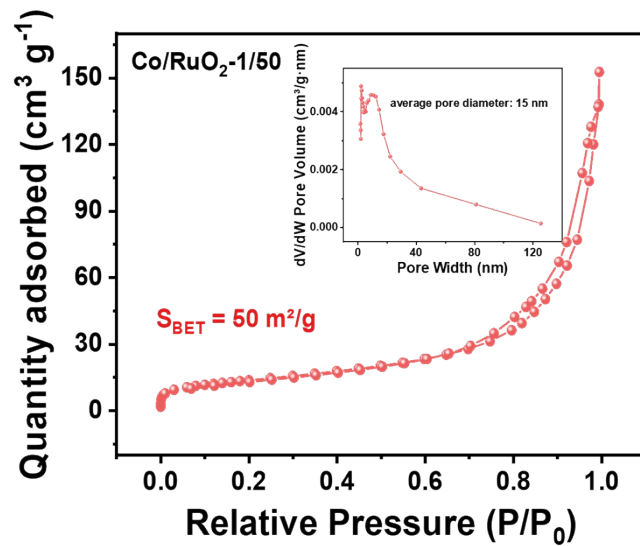


Figure S11. Nitrogen adsorption-desorption isotherms (inset: the pore diameter distribution curve) of $\text{Co}/\text{RuO}_2\text{-1/50}$.

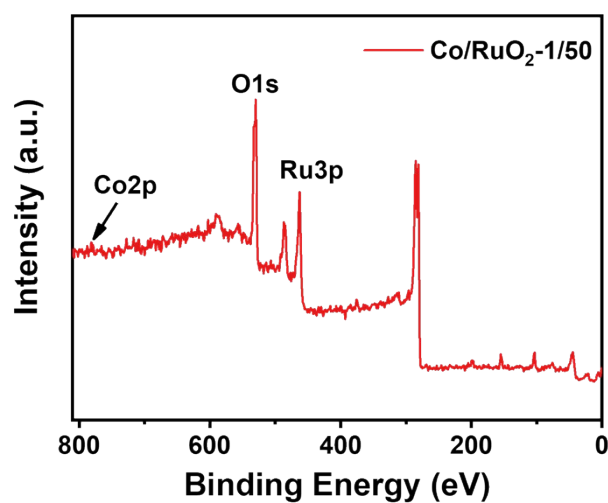


Figure S12. The XPS survey spectrum of Co/RuO₂-1/50.

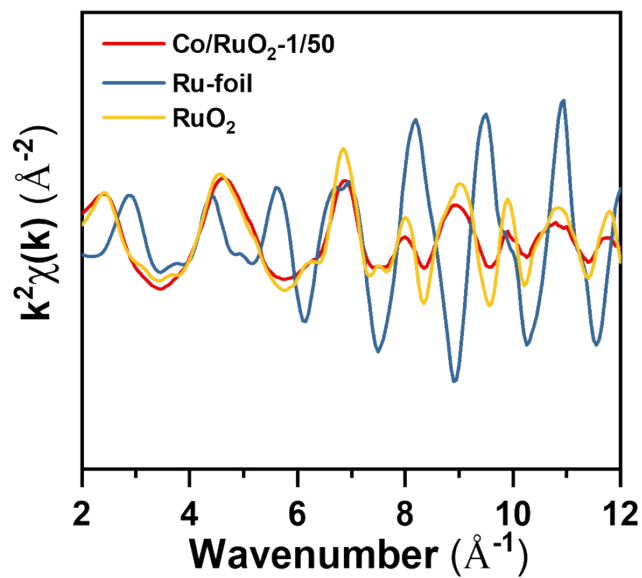


Figure S13. Ru K-edge EXAFS oscillations for Co/RuO₂-1/50, RuO₂ and Ru foil.

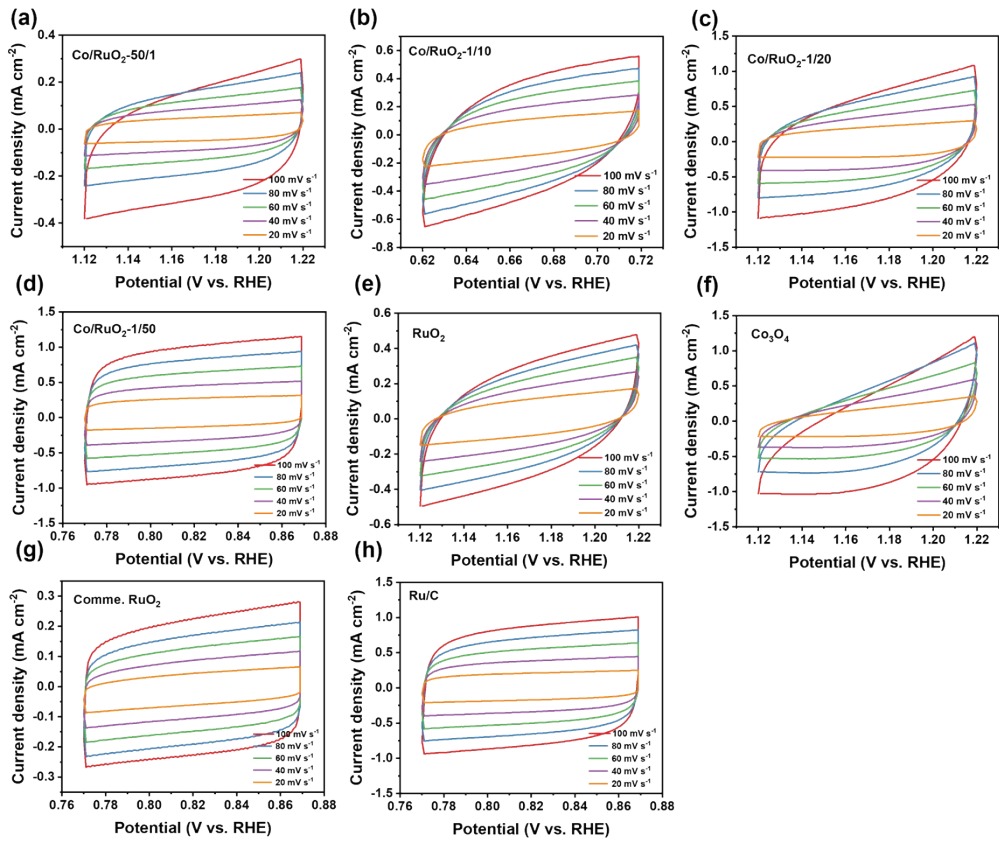


Figure S14. CVs of (a) Co/RuO₂-50/1, (a) Co/RuO₂-1/10, (b) Co/RuO₂-1/20, (c) Co/RuO₂-1/50, (d) RuO₂, (e) Co₃O₄, (f) commercial RuO₂, and (a) Ru/C at varied scan rates (20, 40, 60, 80, 100 mV s^{-1}).

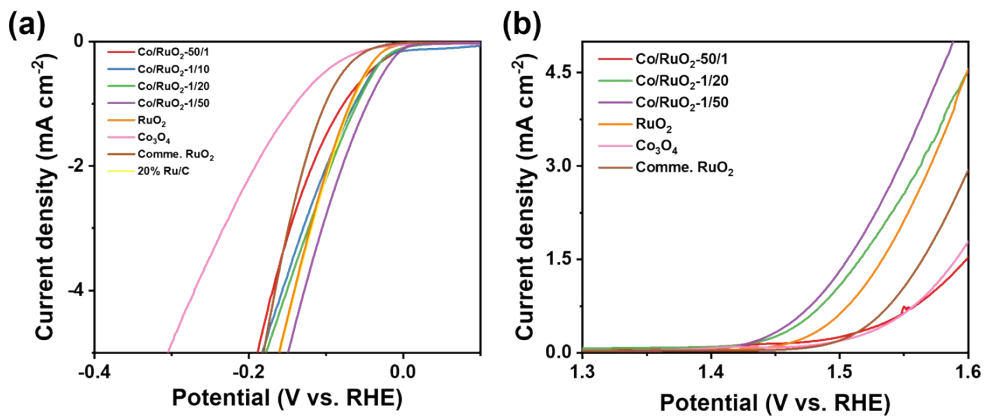


Figure S15. ECSA-normalized LSV curves of samples in 1 M KOH. (a)HER, (b) OER.

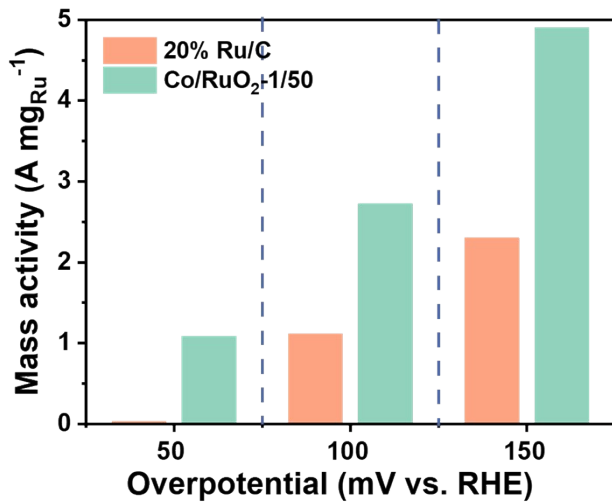


Figure S16. The mass activities of Ru element for Co/RuO₂-1/50 and 20% Ru/C toward HER process.

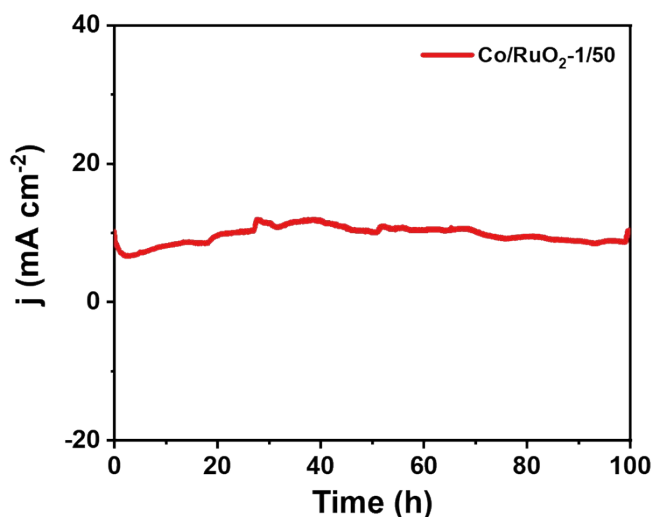


Figure S17. I-t curve for Co/RuO₂-1/50 at 10 mA cm^{-2} in 1 M KOH.

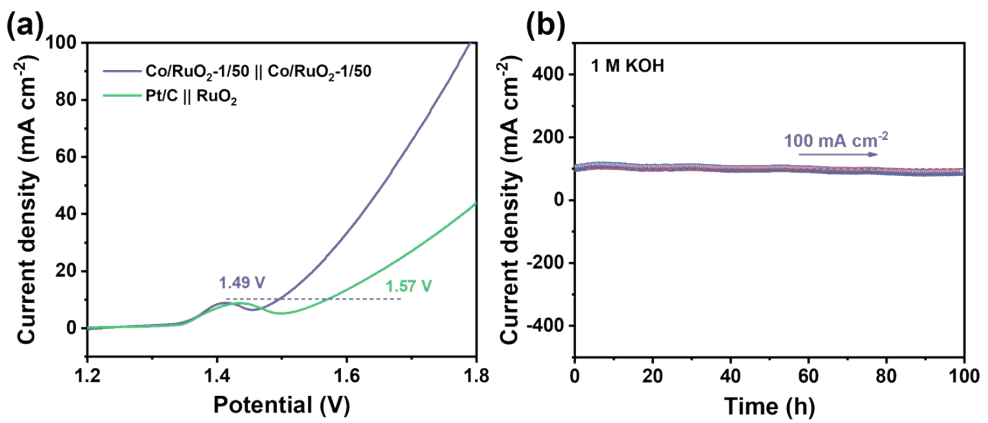


Figure S18. (a) LSV curves of water electrolysis in alkaline environment. (b) i-t stability test curve of water electrolysis in alkaline environment.

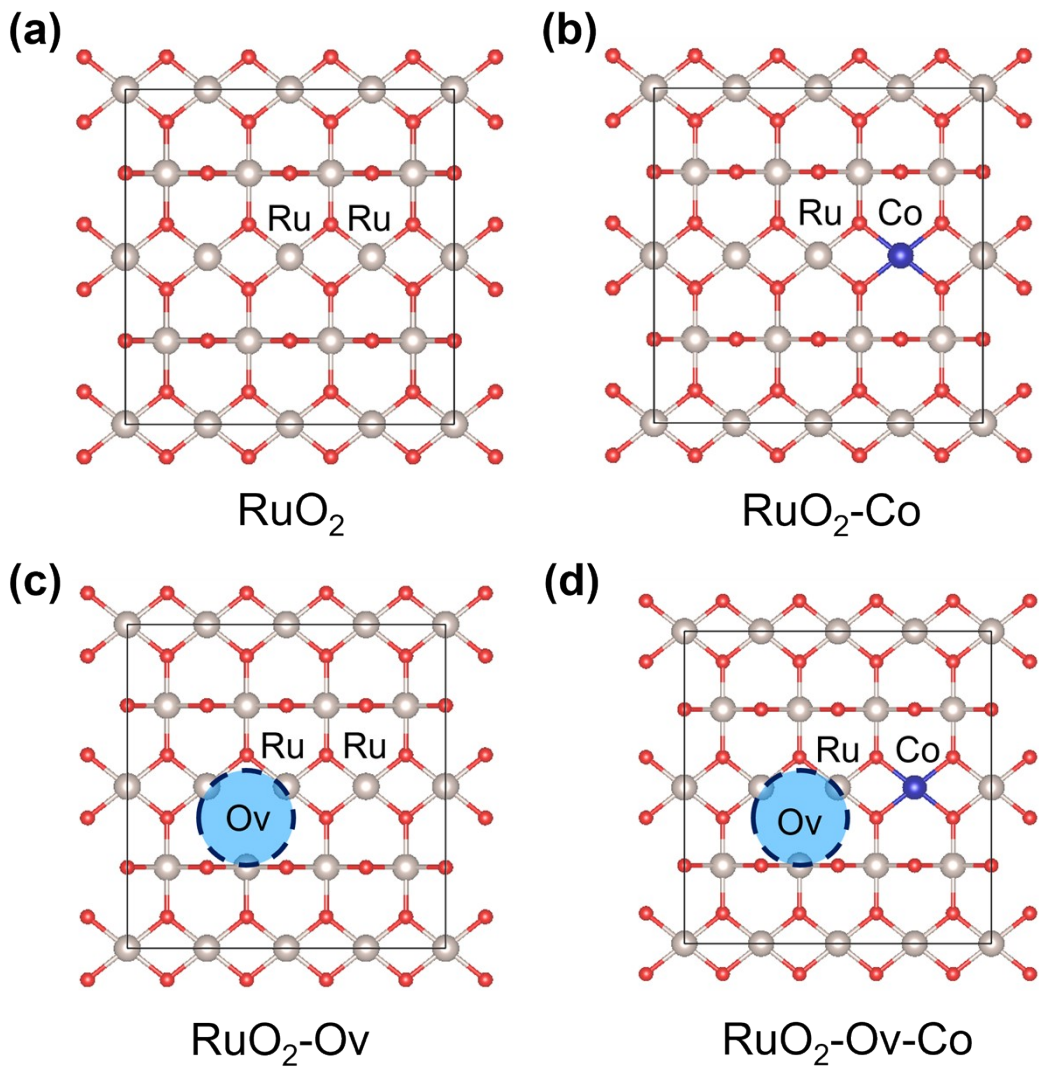


Figure S19. Schematic diagram of the model structure.

Table S1. EXAFS fitting parameters at the Ru K-edge for various samples.

Sample	Shell	CN ^a	R(Å) ^b	$\sigma^2(\text{\AA}^2)$ ^c	ΔE_0 (eV) ^d	K-range /Å ⁻¹	R-range /Å	R factor
Ru foil	Ru-Ru	12*	2.68	0.0039	-4.7	4.0-13.0	1.0-3.0	0.0048
	Ru-O	6.0	1.97	0.0013	-0.4			
RuO ₂	Ru-Ru	9.1	3.14	0.0089	-3.7	2.2-12.0	1.0-3.8	0.0105
	Ru-Ru	5.1	3.59	0.0006	5.3			
	Ru-O	5.6	1.98	0.0035	-0.3			
Co/RuO ₂ -1/50	Ru-O-Co	0.7	3.00		0.0129	-3.8	2.2-12.0	1.0-3.8
	Ru-Ru	8.3	3.13					0.0062
	Ru-Ru	2.4	3.58	0.0018	3.3			

^aCN, coordination number; ^bR, the distance to the neighboring atom; ^c σ^2 , Debye-Waller factor , the Mean Square Relative Displacement (MSRD); ^d ΔE_0 , inner potential correction; R factor indicates the goodness of the fit. S02 was fixed to 0.853, accourding to the experimental EXAFS fit of Ru foil by fixing CN as the known crystallographic value. * This value was fixed during EXAFS fitting, based on the known structure of Ru. Error bounds that characterize the structural parameters obtained by EXAFS spectroscopy were estimated as CN ± 20%; R ± 1%; σ^2 ± 20%; ΔE_0 ± 20%. A reasonable range of EXAFS fitting parameters: 0.700 < S02 < 1.000; CN > 0; σ^2 > 0 Å²; | ΔE_0 | < 15 eV; R factor < 0.02.

Table S2. Comparison of HER performance in 1M KOH of Co/RuO₂-1/50 with previously reported RuCo-based catalysts. (η_{10} : Overpotential at 10 mA cm⁻², mV. b: Tafel slope, mV dec⁻¹)

Catalysts	η	b	Reference
Co/RuO ₂ -1/50	26	54	This work
Co-SAC/RuO ₂	45	58	1
RuO ₂ @Co ₃ O ₄	90	103	2
Ru/Co ₃ O ₄ NWs	31	70	3
Ru/Co(OH) ₂ NWAs	96	68	4
Ru@RuO ₂	137	113	5

Table S3. The actual Ru amount of Co/RuO₂-1/50 by ICP-MS.

Metal	Wt%
Ru	60.7
Co	1.3

Table S4. Comparison of OER performance in 1M KOH of Co/RuO₂-1/50 with previously reported Ru-based catalysts. (E: Potential at 10 mA cm⁻², V. b: Tafel slope, mV dec⁻¹)

Catalysts	E	b	Reference
Co/RuO ₂ -1/50	1.47	88.0	This work
IW-Co ₃ O ₄ -RuO ₂ -HS	1.48	55.4	6
1-RuO ₂ /CeO ₂	1.58	74.0	7
Ru@RuO ₂	1.55	86.0	8
Ru-RuP _x -Co _x P	1.52	85.4	9

CoCrRu LDHs	1.51	56.1	10
Ru@g-CN _x	1.51	49.5	11
Ru/FeCo	1.51	82.8	12
NiCo _{1.7} Ru _{0.3} O ₄	1.51	78.0	13

Table S5. Calculated Gibbs free energies (G) of adsorption species for HER on different catalysts' surfaces (in eV).

	RuO₂	RuO₂-Co	RuO₂-Ov	RuO₂-Ov-Co
*H₂O	-0.61	-0.637	-0.527	-0.503
*H+*OH	0.361	0.114	-0.014	-0.357
*H	0.438	0.184	0.42	0.165

Table S6. The correction of zero-point energy (ZPE) of adsorption species on different catalysts' surfaces (in eV). All the slab atoms were fixed during the vibrational analyses. (T =

298.15 K)

	RuO₂	RuO₂-Co	RuO₂-Ov	RuO₂-Ov-Co
*H₂O	0.65	0.63	0.66	0.64
*H+*OH	0.54	0.51	0.53	0.53
*H	0.17	0.18	0.17	0.16

Table S7. The correction of entropy (TS) of adsorption species on different catalysts' surfaces (in eV). All the slab atoms were fixed during the vibrational analyses. (T = 298.15 K)

	RuO₂	RuO₂-Co	RuO₂-Ov	RuO₂-Ov-Co
*H₂O	0.16	0.15	0.15	0.16

*H+*OH	0.09	0.09	0.08	0.07
*H	0	0	0	0

Supplemental References

1. Shah, K., Dai, R. Y., Mateen, M., Hassan, Z., Zhuang, Z. W., Liu, C. H., Israr, M., Cheong, W. C., Hu, B. T., and et al. (2022). Cobalt Single Atom Incorporated in Ruthenium Oxide Sphere: A Robust Bifunctional Electrocatalyst for HER and OER. *Angew. Chem. Int. Ed.* **61**, e202114951.
2. Jiang, Y., Liu, H., Jiang, Y. M., Mao, Y. N., Shen, W., Li, M., He, R. X. (2023). Adjustable heterointerface-vacancy enhancement effect in RuO₂@Co₃O₄ electrocatalysts for efficient overall water splitting. *Appl. Catal. B-Environ.* **324**, 122294.
3. Liu, Z., Zeng, L. L., Yu, J. Y., Yang, L. J., Zhang, J., Zhang, X. L., Han, F., Zhao, L. L., Li, X., Liu, H., Zhou, W. J. (2021). Charge redistribution of Ru nanoclusters on Co₃O₄ porous nanowire via the oxygen regulation for enhanced hydrogen evolution reaction. *Nano Energy.* **85**, 105940.
4. Han, X., Li, Y. J., Wang, X., Dong, J. T., Li, H. M., Yin, S., Xia, J. X. (2024). Ru anchored on Co(OH)₂ nanowire arrays as highly effective electrocatalyst for full water splitting. *Int. J. Hydrogen Energ.* **51**, 769e776.
5. Zhang, J. T., Ren, G. M., Li, D. Y., Kong, Q. Y., Hu, Z. W., Xu, Y., Wang, S. L., Wang, L., Cao, M. F., Huang, X. Q. (2022). Interface engineering of snow-like Ru/RuO₂ nanosheets for boosting hydrogen electrocatalysis. *Sci. Bull.* **67**, 2103–2111.
6. Gao, Y. X., Zheng, D. B., Li, Q. C., Xiao, W. P., Ma, T. Y., Fu, Y. L., Wu, Z. X., Wang, L. (2022). 3D Co₃O₄-RuO₂ Hollow Spheres with Abundant Interfaces as Advanced Trifunctional Electrocatalyst for Water-Splitting and Flexible Zn-Air Battery. *Adv. Funct. Mater.* **32**, 2203206.

7. Galani, S. M., Mondal, A., Srivastava, D. N., Panda, A. B. (2020). Development of RuO₂/CeO₂ heterostructure as an efficient OER electrocatalyst for alkaline water splitting. *Int. J. Hydrogen Energ.* **45**, 18635e18644.
8. Jiang, R. Z., Tran, D., Li, J. T., Chu, D. (2019). Ru@RuO₂ Core-Shell Nanorods: A Highly Active and Stable Bifunctional Catalyst for Oxygen Evolution and Hydrogen Evolution Reactions. *Energy Environ. Mater.* **2**, 201–208.
9. Wang, L., Zhou, Q., Pu, Z. H., Zhang, Q., Mu, X. Q., Jing, H. Y., Liu, S. L., Chen, C. Y., Mu, S. C. (2018). Surface reconstruction engineering of cobalt phosphides by Ru inducement to form hollow Ru-RuPx-CoxP pre-electrocatalysts with accelerated oxygen evolution reaction. *Nano Energy.* **53**, 270-276.
10. Dong, C. L., Zhang, X. L., Xu, J., Si, R., Sheng, J., Luo, J., Zhang, S. N., Dong, W. J., Li, G. B., Wang, W. C., Huang, F. Q. (2020). Ruthenium-Doped Cobalt–Chromium Layered Double Hydroxides for Enhancing Oxygen Evolution through Regulating Charge Transfer. *Small.* **16**, 1905328.
11. Gao, T. Y., Kumar, K. S., Yan, Z., Marinova, M., Trentesaux, M., Amin, M. A., Szunerits, S., Zhou, Y., Martin-Diaconescu, V., Paul, S., Boukherroub, R., Ordomsky, V. (2023). Covalent organic framework derived synthesis of Ru embedded in carbon nitride for hydrogen and oxygen evolution reactions. *J. Mater. Chem. A.* **11**, 19338.
12. Gao, L., Zhong, X., Chen, J. N., Zhang, Y., Liu, J., Zhang, B. S. (2023). Optimizing the electronic structure of Fe-doped Co₃O₄ supported Ru catalyst via metal-support interaction boosting oxygen evolution reaction and hydrogen evolution reaction. *Chinese Chem. Lett.* **34**, 108085.
13. Peng, C. L., Liu, H., Chen, J. F., Zhang, Y. X., Zhu, L. Y., Wu, Q. M., Zou, W., Wang, J. L., Fu, Z. P., Lu, Y. L. (2021). Modulating the potential-determining step in oxygen evolution reaction by regulating the cobalt valence in NiCo₂O₄ via Ru substitution. *Appl. Surf. Sci.* **544**, 148897